A Tunable Differential Duplexer in 90nm CMOS

Sherif H. Abdelhalem[1], Prasad S. Gudem[2], and Lawrence E. Larson[1,3]

[1]University of California at San Diego, La Jolla, CA 92093, [2]Qualcomm Inc., San Diego, CA 92121,
[3]Brown University, Providence, RI 02912

***Abstract* — An integrated duplexer for frequency division duplex wireless standards around 2GHz is presented. The duplexer utilizes a differential version of a planar hybrid transformer to enable wideband differential to differential and differential to common-mode isolation between the transmitter and receiver. It covers WCDMA bands I, II, III, and IX, with worst-case isolation of 60dB and 40dB at the TX and RX frequencies respectively. The duplexer with a cascaded LNA achieves a noise figure of 5.6dB, and 14dB of gain. The insertion loss in the TX path is 3.7dB. The duplexer and LNA, implemented in a 90nm CMOS process, consume 20mA and occupy an active area of 0.6mm^2.**

***Index Terms* — Cellular phones, CMOS process, tunable circuits and devices, duplexers, WCDMA.**

I. Introduction

Multiband transceivers require a highly integrated solution for cost reduction. Currently, for each supported band, an off-chip duplexer based on highly frequency selective filtering, and a switch to switch between different bands, are used. This adds to the system cost and complexity and a strong need for an integrated approach exists.

In [1],[2] an integrated duplexer based on electrical balance, rather than frequency selective filtering, was introduced, with the topology in [2] offering wider isolation bandwidth. A drawback of that technique is that the PA signal couples as a common-mode signal to the differential LNA inputs. At high PA output powers, this common-mode signal can cause problems ranging from linearity issues to LNA device breakdown.

In this paper, a differential version of the hybrid transformer will be presented to cancel the common-mode coupling and allow reliable high power operation. Section II introduces the idea of the differential duplexer and compares its performance to the single-ended version. The design of the hybrid transformer and LNA implementation details are covered in Section III. Section IV shows the measurement results and Section V concludes the paper.

II. Differential Duplexer Architecture

An integrated duplexer based on a hybrid transformer uses electrical balance to achieve isolation between two of its ports [1]. In Fig. 1(a) the single-ended version from [2] is shown; when the balance impedance equals the antenna impedance, the PA signal appears as an equal swing on the antenna and balance sides, and ideally no signal couples to the LNA side. However the unavoidable capacitive coupling between the primary and secondary windings of the transformer will cause a portion of the PA signal to couple as a common-mode signal to the LNA side [3]. This common-mode swing can be large enough at high PA powers to cause severe linearity issues for the receiver. In the extreme case where an autotransformer, i.e. a center tapped inductor, is used as a hybrid for lower loss [2], the entire PA signal appears at the LNA inputs potentially causing oxide breakdown of the LNA devices.

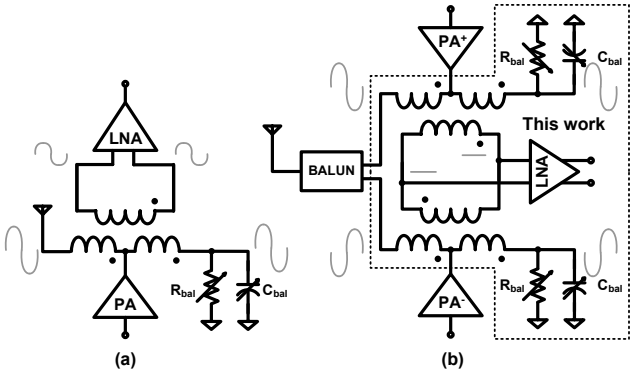

Fig. 1. (a) Single-ended Duplexer [2] (b) Proposed Differential Duplexer.

It should be mentioned that an AC grounded center tap in the secondary windings of a hybrid transformer can reduce the common-mode signal coupled to the LNA, by reducing the common-mode impedance seen on that side. But a zero common-mode impedance is not possible, due to the less than unity magnetic coupling between the two halves of the windings. Another possible solution would be to place a common-mode trap on the LNA side, but such a solution is inherently narrowband, hindering the possibility of a wideband tunable duplexer.

Our proposal to achieve wideband cancellation of the common-mode signal is shown in Fig. 1(b). It relies on a differential PA, so that coupling from one phase of the PA will cancel that from the other phase. This topology brings the advantage of a fully differential transmit and receive path, and adds 3dB to the PA maximum output power for same voltage operation. The clear disadvantage of this is the added balun at the antenna port, whose loss adds to the

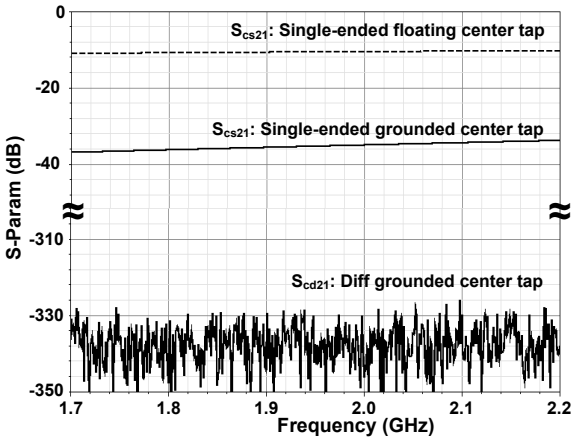

Fig. 2. Comparison of simulated common-mode coupling for differential and single-ended duplexers.

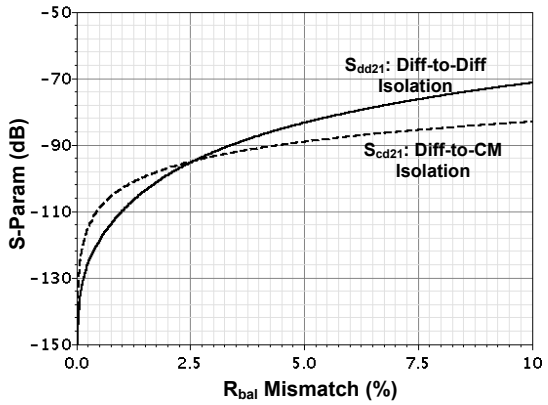

Fig. 3. Balance resistor mismatch effect on differential-to-differential and differential to common-mode isolation.

TX insertion loss and RX noise figure.

Fig. 2 shows simulation results for different topologies. For the comparison, mixed-mode s-parameters were used [4]. Single-ended to common-mode isolation, S_{cs21}, for the duplexer in Fig. 1(a) is compared to differential to common-mode isolation, S_{cd21}, for duplexer in Fig. 1(b), where port 1 is the PA and port 2 is the LNA. A grounded center tap on the secondary windings somewhat improves isolation, while the fully-differential duplexer results in great improvement. Although perfect isolation is only possible with perfect symmetry, simulation results in Fig. 3 with balance impedance mismatch show that with even a 10% mismatch, the isolation exceeds 70dB. This result means that the same control signals can be used for both sides of the balance impedance, to set its nominal value to that of the antenna impedance, and thus achieve electrical balance as in the single-ended version.

A common linearity test to assess the receiver linearity in the presence of TX leakage is the triple-beat (TB) test.

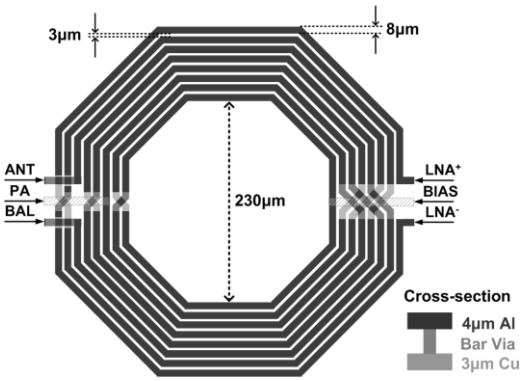

Fig. 4. Hybrid transformer layout. Two of these are required for the proposed duplexer.

A two-tone signal is injected at the PA port and a blocker is injected at the antenna, and then the resulting cross modulation is observed. The cross modulation is proportional to the square of the TX signal leaked into the LNA; thus common-mode and differential leakage are equally problematic. An improvement of 43dB in triple beat ratio (the ratio between jammer and cross modulation at the output) is observed in simulation by employing the differential duplexer rather than the single-ended one.

III. 90nm CMOS Implementation

A. Hybrid Transformer

Fig. 4 shows the layout of the hybrid transformer. To reduce metal resistive losses, the two thick top metal layers, a 4µm thick Aluminum and a 3µm thick Copper, were stacked together with a bar via. A 2:6 turns ratio was chosen to minimize the LNA noise contribution. The primary and secondary windings were interwound and a minimum turns spacing of 3µm was used to maximize magnetic coupling [3]. Turn width and outer radius were optimized by Momentum EM simulations to provide a compromise between metal loss and self resonance frequency, and an 8µm width together with a 200µm outer radius was found to give the lowest loss.

B. LNA

Fig. 5 shows the LNA schematic. A differential pair with cascode devices was used. The LNA device size was optimized with the duplexer for noise figure, and the bias current was optimized for linearity. A portion of the power gain was traded-off for improved noise, so the duplexer provides an impedance to the LNA that is closer to a noise match than a power match. The LNA output was matched to 50Ω for ease of measurement, and a three bit bank of capacitors was used to center the gain curve at the required receive band.

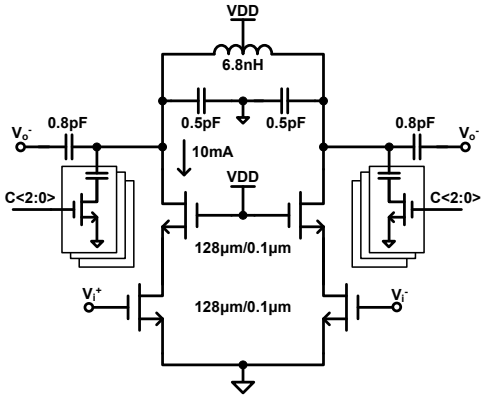

Fig. 5. LNA schematic.

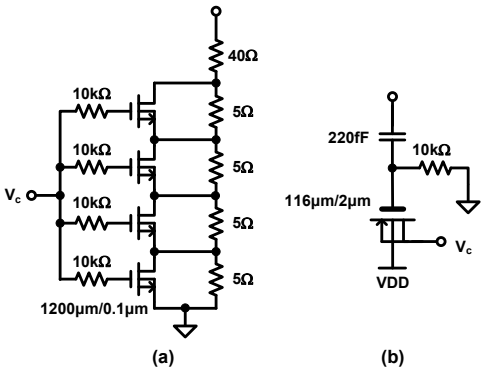

Fig. 6. Balance network schematic, (a) voltage controlled resistor (VCR) (b) voltage controlled capacitor (VCC).

C. Balance Network

The balance between the antenna impedance and the balance impedance is very critical to obtain the required isolation. An on-board tunable open stub together with the bondwire inductance and pad capacitance provides a nearly 50Ω antenna impedance to the duplexer. On the balance side, a voltage controlled resistor (VCR) in parallel with a voltage controlled capacitor (VCC) was used.

As shown in Fig. 6(a), the VCR can vary from roughly 40 to 60Ω. To withstand high powers, the variable part was split into four series components to divide the voltage swing among them, and an RF floating gate was utilized so that voltage swing splits between V_{gs} and V_{gd}. Fig. 6(b) shows the VCC, it varies between 150 and 200fF. A series MIM capacitor was used to reduce the voltage swing across the varactor, which was implemented with an inversion mode thick oxide MOS varactor.

It should be mentioned that analog control of the balance impedance can ideally provide perfect balance with the antenna impedance without the quantization steps of a digital alternative, but it also makes the optimum

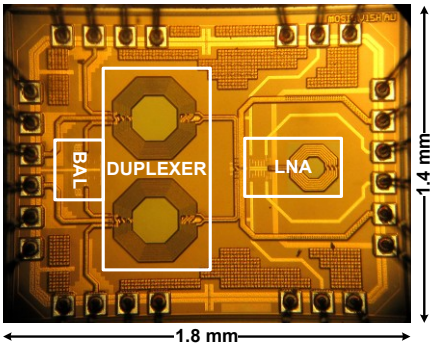

Fig. 7. Die microphotograph.

control voltages power level dependent. It may also cause some nonlinearity, which would leak back into the LNA and potentially degrade receiver linearity. That is why the range of analog variability should be kept to minimum, and may ideally be combined with other digital controls to maximize the covered range.

IV. Measurement Results

Fig. 7 shows the die photo. Implemented in a 90nm CMOS process, the active area is 0.6mm^2. The die was packaged in a 24pin QFN plastic package and mounted on a FR4 board for testing.

Fig. 8 shows the measured TX to RX isolation. Differential to differential isolation of more than 70dB can be achieved at any channel between 1.7 and 2.2GHz. The isolation at the receive band is better than 40dB for the worst case spacing of 190MHz between the transmit and receive bands (IMT case). Differential to common-mode isolation better than 60dB was measured. Fig. 9 shows the measured cascaded noise figure and gain of the duplexer followed by the LNA, more than 14dB of gain is achieved across the receive bands with a noise figure ranging from 5.2 to 5.9dB. Fig. 10 shows the measured return loss at the PA port and the insertion loss from the PA to the antenna. The insertion loss, including 0.2dB board loss, was less than 3.9dB.

The high power measurement was carried out using external baluns, and balun loss was dembedded from the results. Isolation with TX powers up to 27dBm was verified. Fig. 11 shows the LNA output spectrum in a triple-beat test. Two tones with 27dBm of power were applied to the PA port with a center frequency of 1.95GHz and 5MHz spacing, a single-tone jammer of -43dBm at 2.14GHz was applied to the antenna port, and the resulting cross modulation at 2.145GHz was observed at the LNA output. The measured triple beat ratio was 58.2dB. The receiver IIP3 measured in a two-tone test was -5.6dBm, implying that duplexer isolation (ISOL=TB/2+P_{TX}-IIP3) is effectively 61.7dB.

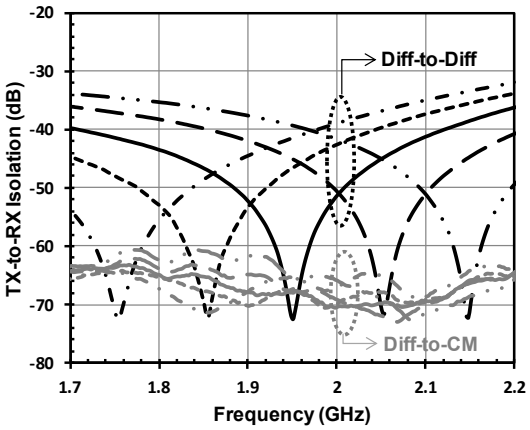

Fig. 8. Measured differential-TX to differential-RX isolation and differential-TX to common-mode-RX isolation.

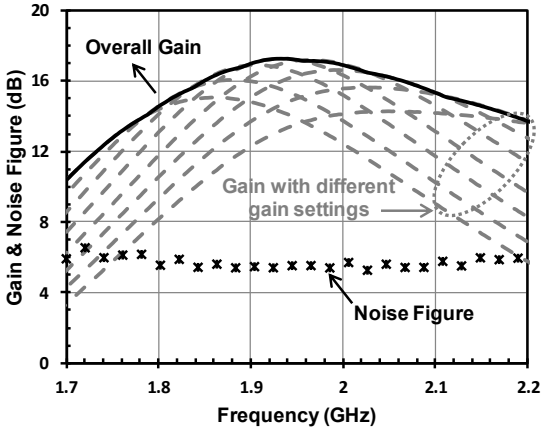

Fig. 9. Measured cascaded gain and noise figure of duplexer and LNA.

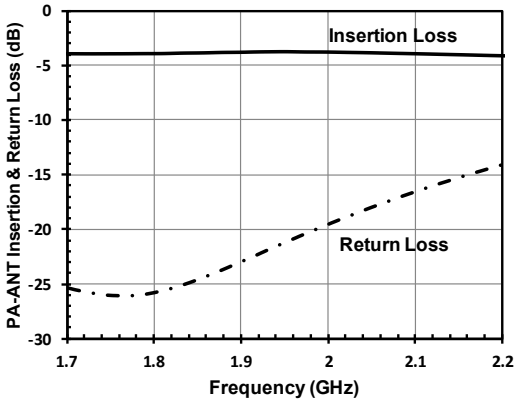

Fig. 10. Measured TX insertion and return loss.

V. Conclusion

A technique to achieve wideband differential and common-mode isolation in integrated duplexers based on hybrid transformers was introduced. This technique enables high transmit powers and significantly improved cross-modulation performance. The performance of the duplexer is summarized and compared to other state-of-the-art implementations in Table 1.

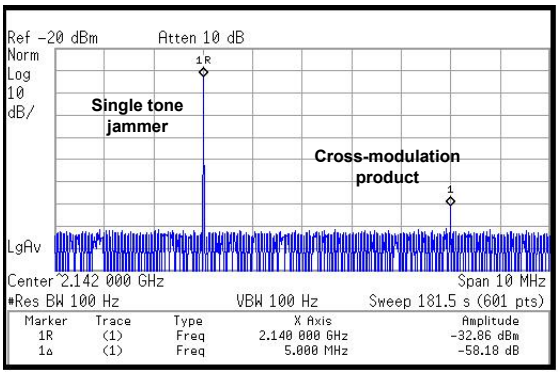

Fig. 11. Measured spectrum from triple beat test (P_{TX} = 27dBm, P_{jammer} = -43dBm).

TABLE I
COMPARISON WITH STATE-OF-THE-ART

Parameter			Murata SAYRF1G95CA0B0A	Ref[2]	This Work
Technology			SAW	65nm CMOS	90nm CMOS
# Bands Covered			1	4	4
High Power			Yes	No	Yes
ISOL	TX Band	DM	57dB	55dB	70dB
		CM	45dB	0dB	60dB
	RX Band		50dB	45dB	40dB
TX IL			1.6+1.1† = 2.7dB	2.5dB	3.9dB
Casc. RX NF			2.4+1.1† +2*= 5.5dB	5dB	5.9dB
Area (mm^2)			3.2	0.1	0.6

†Assumes Skyworks SKY13380-350LF SP4T switch and 0.3dB board loss.
*Typical LNA NF.

References

[1] M. Mikhemar, H. Darabi, and A. Abidi, "A tunable integrated duplexer with 50dB isolation in 40nm CMOS," *ISSCC Dig. Tech. Papers*, pp. 386-387, Feb.2009.

[2] M. Mikhemar, H. Darabi, and A. Abidi, "An on-chip wideband and low-loss duplexer for 3G/4G CMOS radios," *VLSI Symp. Dig.*, pp. 129-130, June 2010.

[3] J. Long, "Monolithic transformers for silicon RFIC design," *IEEE J. Solid-State Circuits*, vol.35, no. 9, pp. 1368-1382, Sep. 2000.

[4] D. Bocklemann, and W. Eisenstadt, "Combined differential and common-mode scattering parameters: theory and simulation," *IEEE Trans. Microwave Theory & Tech.*, vol. 43, no. 7, pp. 1530-1539, July 1995.